AIAA Propulsion and Energy Forum
19-22 August 2019, Indianapolis, IN
AIAA Propulsion and Energy 2019 Forum

10.2514/6.2019-4294

Linear Burn Rate of Ionic Liquid Multimode Monopropellant

Nicolas Rasmont,[1] Emil J. Broemmelsiek,[1] Alex J. Mundahl,[1] and Joshua L. Rovey[2]
University of Illinois Urbana-Champaign, Urbana IL, 61801

Multimode microthrusters are capable of both high specific impulse electrical operation and high thrust chemical operation, allowing a high degree of mission flexibility for small satellites. This technology requires a monopropellant capable of sustaining both modes of propulsion, through catalytic exothermic decomposition (chemical mode) and electrospray (electric mode). Previous research has identified a double-salt ionic liquid consisting of 41% wt. 1-ethyl-3-methylimidazolium ethyl sulfate and 59% wt. hydroxylammonium nitrate as a promising propellant candidate. The objective of this work is to measure its linear burn rate. The burn rate is measured through pressure-based and high-speed imaging methods in a fixed-volume pressurized reactor across a pressure range from 0.5 to 10 MPa. Its performance is compared to benchmarks 80% wt. hydroxylammonium nitrate-water and nitromethane propellants, both of which show good agreement with the literature. The burn rate of the multimode monopropellant is found to follow an exponential law $r_b = 5.35e^{1.11P}$ between 0.5 and 3 MPa and being approximately constant at 140 mm/s between 3 and 10 MPa.

Nomenclature

r_b	=	Linear burn rate (mm/s)
D_c	=	Diameter of propellant container (mm)
V	=	Volume of propellant (mL)
Δh	=	Change in height (mm)
Δt	=	Change in time (s)
P	=	Pressure (MPa)
a	=	Burn rate coefficient (mm/s)
n	=	Burn rate exponent (unitless)

I. Introduction

Multimode propulsion is defined as the integration of two distinct propulsive modes on a single spacecraft, generally a high specific impulse, low thrust electric mode and a low specific impulse, high thrust chemical mode. The availability of both propulsion modes offers a high degree of flexibility during the mission design phase, by allowing trajectories and maneuvers that would be impossible otherwise[1]–[5]. The chemical mode is well-suited for time-sensitive maneuvers, such as orbit insertion, rendezvous or debris avoidance, while the electric mode is useful for long, high Δv maneuvers such as orbital stationkeeping and interplanetary transfer. This combination can lead to significant mass savings and shorter transfer time compared to a spacecraft equipped with a single propulsion method. Even greater mass savings can be achieved by sharing propellants and thruster hardware, even if the performances of such a hybrid system are lower in both propulsion modes than two separate but specialized propulsion systems[6], [7]. The use of a common propellant supply allows any combination of maneuvers to be realized before propellant

[1] Graduate Research Assistant, Department of Aerospace Engineering, 317 Talbot Laboratory, 104 S. Wright St.
[2] Associate Professor, Department of Aerospace Engineering, 317 Talbot Laboratory, 104 South Wright St., AIAA Associate Fellow, rovey@illinois.edu.

depletion, enhancing mission flexibility. The benefits of this configuration are particularly significant for small spacecrafts (mass < 50 kg), for which the payload ratio penalty associated with two separate propulsion systems would negate most benefits of multimode propulsion. A promising multimode architecture associates a microtube catalytic thruster with an electric electrospray thruster sharing a common monopropellant[8]–[10]. Both types are based on the use of thin (millimeter-scale width) channels, allowing common thruster hardware to be used for either operation. Previous investigations focused on finding a suitable propellant for this application, and identified a double-salt ionic liquid mixture of 41% 1-ethyl-3-methylimidazolium ethyl sulfate ([Emim][$EtSO_4$]) and 59% hydroxylammonium nitrate by mass (HAN)[11]. It combines high performance in both propulsion modes with a relatively low toxicity, making it an ideal choice for use on a micropropulsion system[8], [11], [12].

The development of this propellant rests on the considerable advances made in electrospray propulsion in recent years[13]. This progress has been driven by the increase in small satellite launches, for which electrospray micropropulsion is particularly well-suited, as the thrust-to-power and thrust-to-weight ratios of such a system are higher than any other electric thruster technology available[14]. For this application, room-temperature ionic liquids (IL) such as [Emim][$EtSO_4$] are ideal propellants, as they have negligible vapor pressure and high electrical conductivity[15]. Because HAN is an ionic compound with a low vapor pressure, an [Emim][$EtSO_4$]-HAN blend is a viable electrospray propellant. Previous analysis[16] showed that [Emim][$EtSO_4$] could react as a fuel with HAN as the oxidizer, with an ideal oxidizer-to-fuel (O/F) ratio of 4 (80% HAN per weight). Catalyst materials impose a limit on propellant flame temperature, which led to the current O/F ratio of 1.44 (59% HAN).

The choice of a HAN-based multimode propellant is the result of recent research efforts focused on finding a suitable replacement for legacy storable propellants. Historically, hydrazine and its derivatives (monomethylhydrazine and unsymmetrical dimethylhydrazine) have been ubiquitous in satellite propulsion systems, either alone as a monopropellant or as a bipropellant in association with nitric acid or nitrogen tetroxide. These propellants have the advantages of being easy to ignite, pose little risk of detonation, and are stable at room temperature [17]. However, their high toxicity and high volatility greatly complicate handling, which increases launch costs[17]–[19].

Among the most promising alternatives to hydrazine currently being developed are energetic ionic compounds, namely hydroxylammonium nitrate (HAN), ammonium dinitramide (ADN) and hydrazinium nitroformate (HNF) [18], [20]–[23]. These salts have highly exothermic decomposition reactions, which allow them to be used as a monopropellant. They are typically blended with additives to enhance specific impulse (fuel compounds, such as methanol or ammonia) and fine tune the physicochemical properties of the propellant (glycerol to lower vapor pressure or water to adjust viscosity and flame temperature). The resulting propellants, such as AF-M315E (HAN-based, developed by the US Air Force Research Laboratory) or LMP-103S (ADN-based, developed by EURENCO-Bofors and ECAPS), have a higher specific impulse and impulse density and lower toxicity than hydrazine[17]. Both are rapidly maturing technologies, with LMP-103S having been successfully tested on the PRISMA ESA mission in 2010 and AF-M315E being tested on the Green Monopropellant Infusion Mission (GPIM) scheduled to launch in June 2019 [24] [25]. These propellants are however not usable in a multimode microtube electrospray thruster, as they contain volatile compounds which would greatly impede electrospray operation.

This paper studies the linear burn rate of [Emim][$EtSO_4$]-HAN propellant for a wide range of pressure relevant to thruster operating conditions. In addition, the linear burn rate of state-of-the-art hydroxylammonium nitrate-water (HAN-water) and nitromethane monopropellants are measured to validate the experimental setup and compare the performance of the [Emim][$EtSO_4$]-HAN propellant. The setup of the experiment is described in Section II, while experimental results are presented in Section III and discussed in Section IV. The conclusions of the study are presented in the Section V.

II. Experimental Method

The experiment described here is similar to previous studies of monopropellant linear burn rate[12], [26]–[29]. In a constant-volume pressurized vessel, a sample of monopropellant is ignited and its linear burn rate measured by monitoring the pressure variation with time inside the chamber and by capturing high-speed images of the burning liquid. These two methods are both used in this work and the results compared, showing excellent agreement.

A. Experimental Setup

A constant-volume pressurized vessel is used for all experiments. The vessel used for this experiment was previously used for [Emim][$EtSO_4$]-HAN burn rate experiments at a lower operating pressure[12]. It has a volume of 1.9 L, a length of 260 mm and diameter of 95.5 mm. To withstand the higher pressure range of this study, a threaded section was added to the lip of the vessel, which ensures a more robust mechanical connection between the vessel and its flange. Photographs with callouts of the components of the experimental setup are shown in Figure 1. Inside the

pressure vessel, a sample of monopropellant is ignited and the pressure variation inside the chamber is measured with a PX309-3KG5V pressure transducer (1), with a gauge pressure range of 0 to 20.7 MPa. An ADS1115 16-bit ADC is used to acquire the sensor data with high accuracy. An SD card module piloted by an Arduino board is used to store the data. High-speed imaging (HSI) of the burn rate is performed using a Chronos 1.4 high-speed camera through a 25.4 mm viewport (2) in the flange of the pressure vessel. The propellant is held in a quartz container (3) made of a 6.02 mm-wide quartz tube epoxied to a 12.7 mm quartz disk acting as its base. The propellant is placed on a platform (4) including two threaded rods (5) acting as electrical connectors (6) for the ignition wire (7), as shown in Figure 1. Ignition is achieved using a 28-gauge diameter nichrome wire dipped in the propellant; for some low-pressure tests, a slug of nitrocellulose (flash paper) is added to increase ignition energy. An LED (8) located inside the pressure vessel illuminates the sample. The pressurant gas is either nitrogen for HAN-based propellants or compressed air for nitromethane, as incandescent wire ignition of nitromethane in an inert atmosphere has been shown experimentally to be extremely difficult[26]–[28].

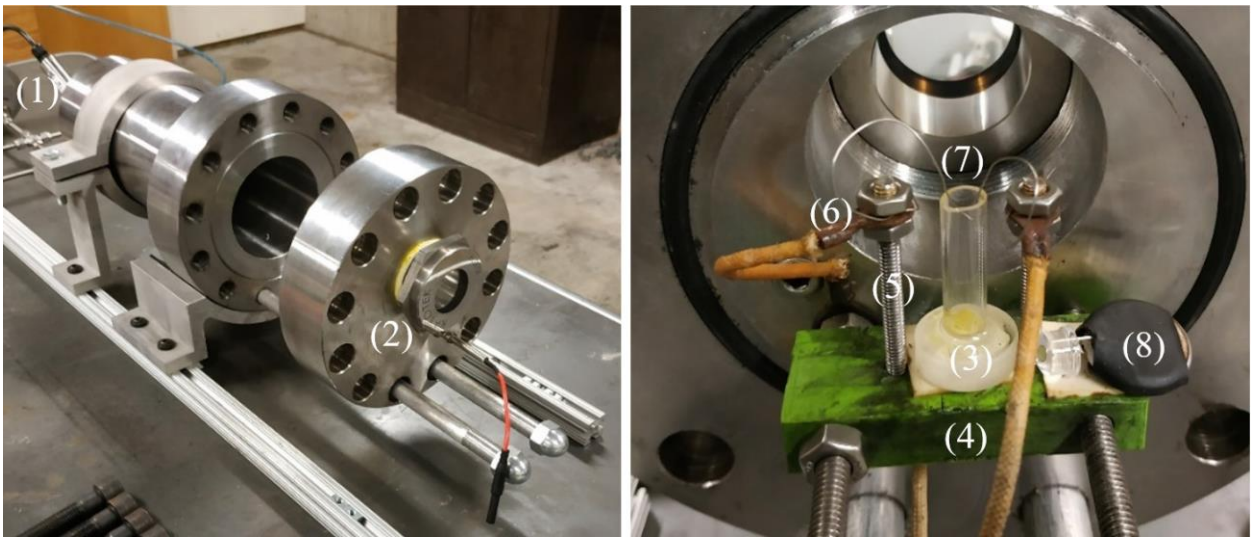

Figure 1. Pressure vessel in open position (left) and details of the propellant holder platform (right)

The experimental procedure starts with filling the sample holder with 0.60 mL propellant using a graduated pipette and securing it on its platform with adhesive tape. A 70-mm-long piece of nichrome wire is cut and its extremities looped around the electrical connector columns. The wire is submerged in the propellant no more than 5% of the total liquid height. The flange is closed and secured to the vessel, and the gas cylinder regulator is set at the desired experimental pressure. The pressurization valve is opened under remote control until the pressure in the chamber stabilizes at the desired level. A BK Precision 1665 power supply is then used to apply a 10A current through the nichrome wire, resistively heating it to a glow until rupture and triggering the ignition of the propellant. Following each test, the combustion gases are vented outside of the laboratory and the experiment can be repeated.

Three different types of propellants were tested. A formulation of [Emim][$EtSO_4$]-HAN propellant with a HAN mass concentration of 59%, corresponding to the current multimode propellant blend, was compared to two benchmarks: a HAN-water solution at a concentration of 80% wt. and nitromethane. These propellant were selected because of their well-explored burn rate behavior[11], [26]–[29] and because they cover the entire range of burn rate (1-400 mm/s) that is expected for HAN-based propellants over the considered pressure domain. HAN-based propellants were manufactured from a commercial 24% by wt. HAN aqueous solution from Sigma-Aldrich with a purity above 99.999%. The solution was first concentrated up to 90% in a rotary evaporator, and the remaining water was eliminated through azeotropic vacuum distillation with isopropyl alcohol, resulting in solid HAN crystals. The crystals were then dissolved in the solvent (distilled water or [Emim][$EtSO_4$]) at the desired concentration. This method is an improvement on previously used synthesis processes [11], [16], as it is more reliable and can be used with larger batches. The [Emim][$EtSO_4$] used for this study was sourced from Sigma-Aldrich with a purity above 95%. The nitromethane was also sourced from Sigma-Aldrich with a purity guaranteed above 98.5%. The pressure range for this study is 0.5 to 11 MPa. The lower part of this range, from 0.5 to 1.5 MPa, is relevant to micropropulsion operation, while the upper part up to 11 MPa provides comparison of our results with burn rate data from the literature.

B. Visual Measurements

High-speed imaging (HSI) provides the height of propellant at any point during the combustion by comparing it with the known external diameter of the propellant holder (8.00 mm). The accuracy of this method is limited by the resolution and contrast of the image, resulting in a relative uncertainty between 2% and 0.5% depending on the duration and distance considered during the acquisition. A Chronos 1.4 high speed camera is used to acquire high-speed (1057 fps) images of the combustion. Knowing the acquisition speed of the camera, the position of the flame front in the holder during the combustion can be plotted as a function of time, and the linear burn rate is defined as the linear correlation coefficient of the dataset obtained. An example of how burn rate is determined from high-speed images for HAN-water propellant is shown in Figure 2.

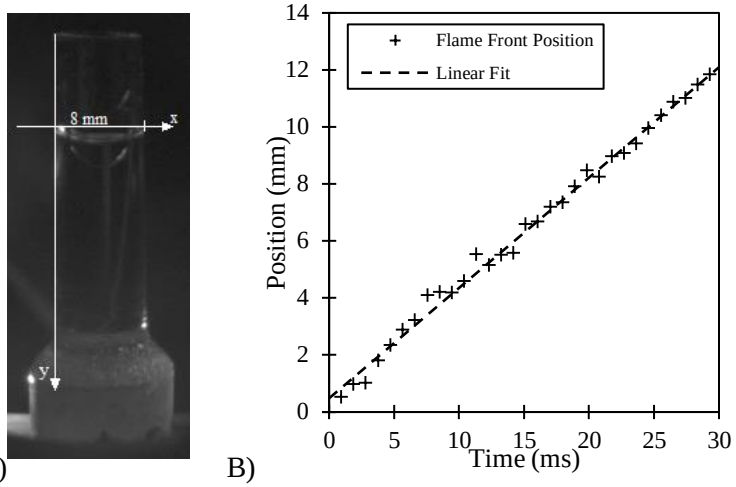

Figure 2. (A) Coordinate selection and (B) example of HSI data (right)

C. Pressure-based Measurement

The temporal evolution of the pressure in the vessel is also used to estimate the propellant burn rate. Assuming a constant burn rate during the combustion and a uniform cross-section in the holder, the burn rate is expressed as the ratio between the change in propellant level in the holder over the burn time, as given in equation (1). This method was used in previous studies[12], [28]. The height of propellant is deduced from the volume of propellant inserted in the holder, which is measured within ±0.01 mL using a graduated pipette. Knowing the internal diameter of the holder, the height of propellant can be calculated. The burn time is deduced by measuring the duration of the pressure rise in the chamber from pressure sensor data. The rate of the acquisition system is 490 Hz, leading to an uncertainty on burn time of ±4 ms.

$$r_b = \frac{\Delta h}{\Delta t} = \frac{4V}{\pi {D_c}^2 \Delta t} \tag{1}$$

A sliding-average filter is used to smooth the signal, with the number of samples adapted to the ignition time scale. The method used to determine the burn time depends on type of propellant studied. Nitromethane and [Emim][$EtSO_4$]-HAN pressure traces show a distinct change of slope at the beginning and end of the combustion, as seen in Figure 3A and Figure 3B, respectively. On the other hand, the pressure trace of HAN-water propellants continues to increase even after all the liquid propellant in the sample holder has been depleted. This behavior was documented by Stahl [28], who showed that the duration of the combustion can be accessed by taking the derivative of the pressure trace. The burn time can be calculated as the time it takes for the pressure trace slope to rise from zero to its maximum, as shown in Figure 3C and Figure 3D. This method shows close agreement with HSI data. The relative measurement error of this method, due to the compounded errors of volume and burn time measurement, decreases when the burn time increases, with a maximum of 12.3% for a burn rate of 476 mm/s and a minimum of 5.0% for a burn rate of 3 mm/s.

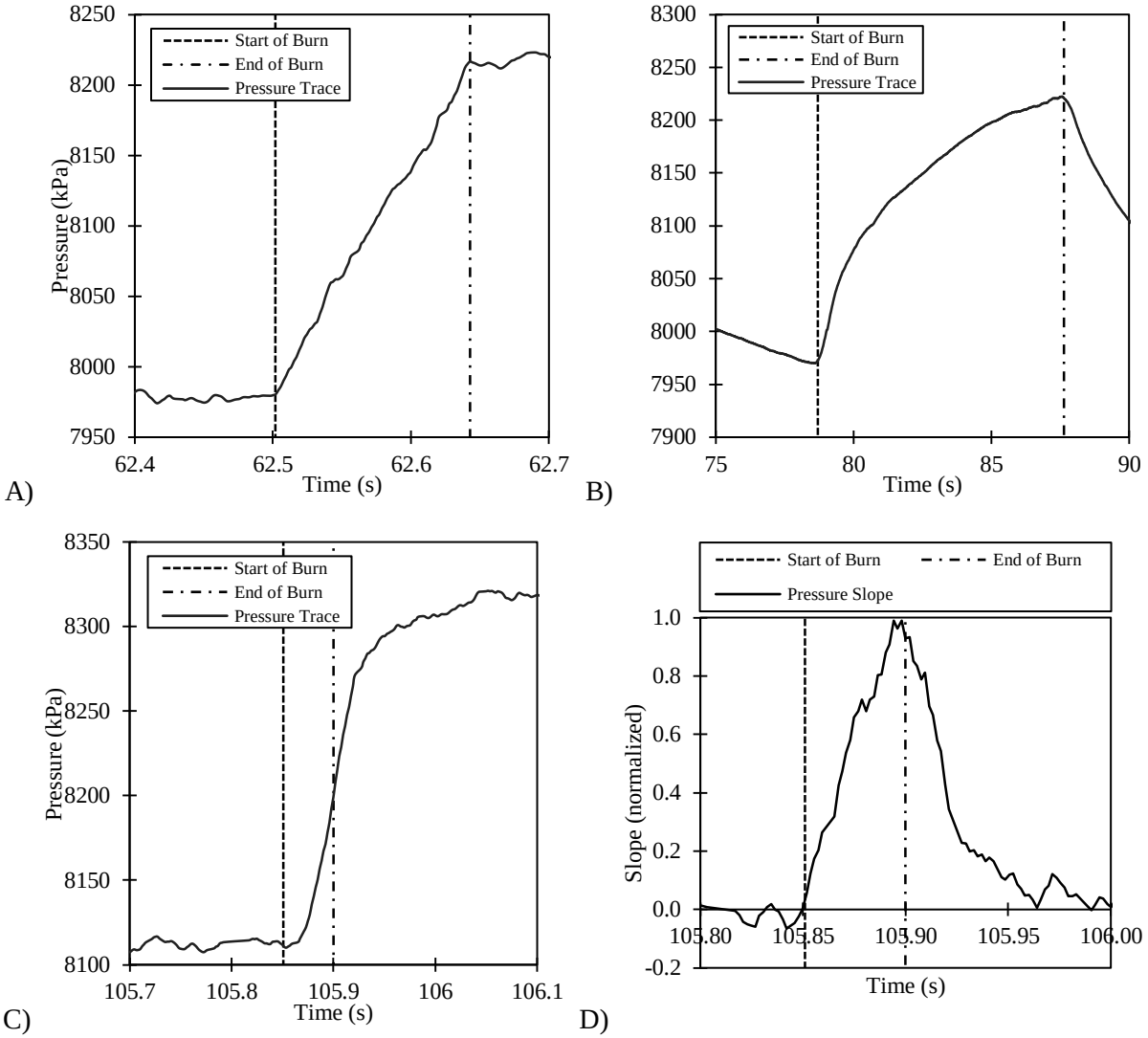

Figure 3. Example pressure traces for (A) [Emim][EtSO$_4$]-HAN, (B) Nitromethane, and (C) 80% wt. HAN-water, and (D) slope of the pressure trace for 80% wt. HAN-water.

III. Results

HAN-based propellant burn rates were acquired at pressures of 0.5, 0.75, 1.0, 1.25, 1.5, 2.0, 3.0, 4.0, 6.0, 8.0 and 10.0 MPa. Previous studies have shown that nitromethane combustion is highly difficult to sustain under 3 MPa [27][28], so the burn rate of nitromethane was acquired at pressures at and above 3 MPa, specifically 3.0, 4.0, 5.0, 6.0, 7.0, 8.0, 9.0, 10.0, and 11.0 MPa. Every burn rate was measured three times for each pressure level to allow the calculation of variances and averages.

A. Nitromethane Linear Burn Rate

The measured burn rates are presented in Figure 4A. It is observed that at high pressure (>9.0 MPa), pressure-based burn rate measurements are systematically higher than HSI-based measurements. This can be explained by the increased burn rate of nitromethane during its violent ignition sequence, which skews the overall burn rate measured by pressure-based method toward higher values than the steady-state burn rate measured by HSI. This effect was not observed for HAN-based propellants, likely because of their lower ignition energy compared to nitromethane. At the lowest pressure investigated here, 3 MPa, the HSI-based burn rate was 0.67±0.03 mm/s against a pressure-based measurement of 0.66±0.01 mm/s. The relative gap between these measurements is 1.5%, within standard deviation. At the largest pressure of 11 MPa, the HSI-based burn rate was 3.05±0.05 mm/s while the pressure-based measurement

was 4.35±0.42 mm/s, a 42% gap. The average standard deviations of HSI and pressure-based measurements are 4.09% and 6.36%, respectively. A strong linear relationship between HSI measurements and pressure is observed in the entire range, with a coefficient of determination of 0.982 for $r_b = 0.307P - 0.203$. Similarly, pressure-based burn rates follow a law $r_b = 0.342P - 0.376$ with a coefficient of determination of 0.986 in the 3.0 to 8.0 MPa range where a linear behavior is observed.

As seen in Figure 4B, the combustion of nitromethane is laminar and exhibits a bright flame and no meniscus or bubble formation is observed. At the mouth of the propellant holder, an unstable flame is observed due to the combustion of decomposition products with oxygen. This does not impact the steady-state burn rate of nitromethane, which is due only to nitromethane decomposition and thus applicable in the context of a monopropellant.

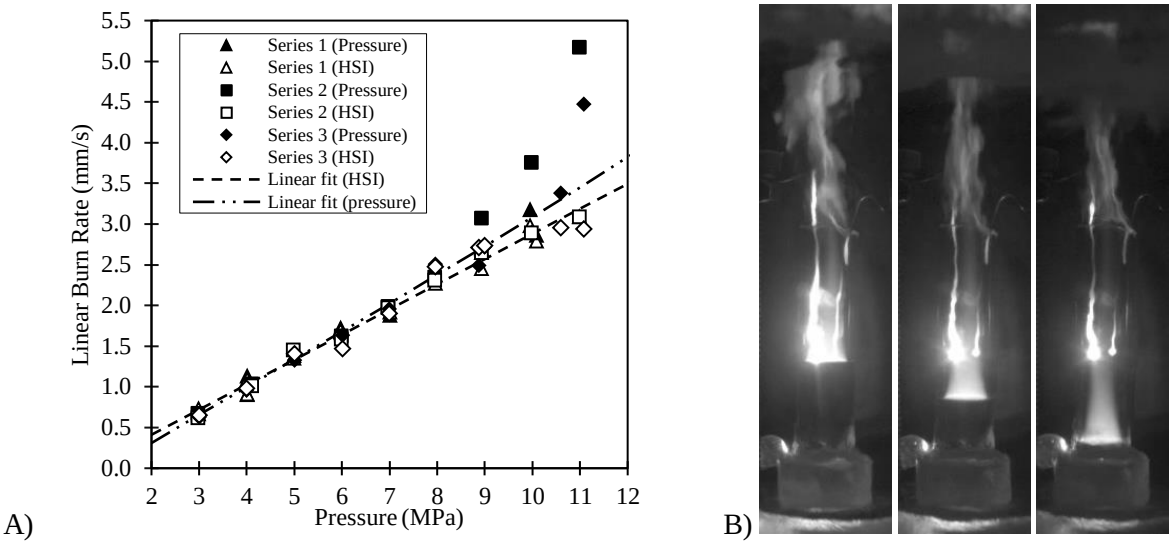

Figure 4. (A) High-speed images of nitromethane decomposition and (B) measured linear burn rate of nitromethane at different pressures.

B. HAN-water Propellant Linear Burn Rate

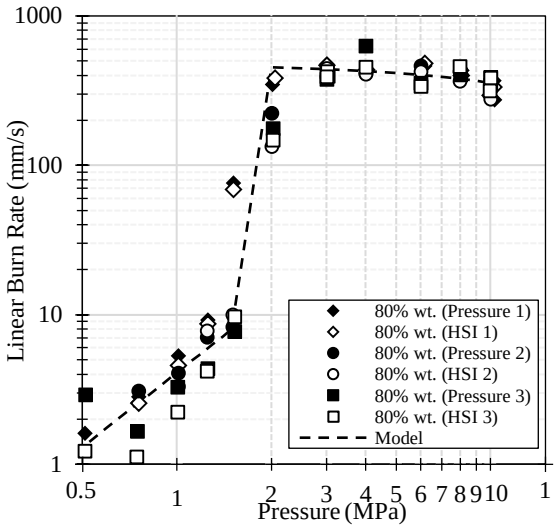

Figure 5. 80% HAN-water linear burn rate results

HAN-water burn rate results are shown in Figure 5 and will be discussed first, followed by discussion of the correlation of the burn rate data with visual observations of the decomposing liquid, gas, and interface. HAN-water burn rate varies between 1-2 mm/s at low pressure (0.5 MPa) and 400-500 mm/s at higher pressure (3.0-10.0 MPa). Three burn rate regions are identified in Figure 5: low, intermediate, and high. These regions appear to correspond with different combustion behavior in each region. The intermediate burn rate corresponds to the transition from low to high burn rate observed between 1.5 and 3.0 MPa. Below 1.5 MPa, the burn rate shows good fit against a power

law $r_b = 4.09P^{1.66}$, with a coefficient of determination of 0.74. Above 3.0 MPa, the burn rate follows a slightly decreasing linear trend $r_b = 478 - 12.30P$ with a coefficient of determination of 0.365. Good agreement between HSI and pressure-based burn rate data is observed with a maximum difference of 16% and an average difference of only 7%. Outside of the intermediate burn rate zone, the standard deviation between the three data points at a specific pressure is low, with a maximum of 28% in the 0.5-1.25 MPa range and 13% between 3.0 and 10.0 MPa. The standard deviation between data points within the intermediate burn rate zone is much higher at 78%. This may be because the transition from low to high burn rate is triggered by random local disturbances in the interface between the liquid and two-phase interface, which can greatly impact the overall burn rate, as described below.

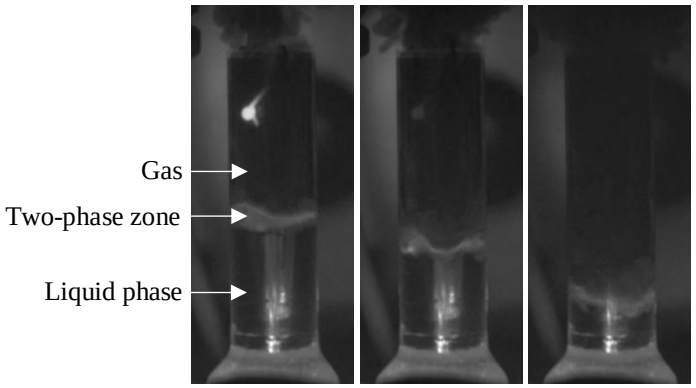

Figure 6. Combustion wave structure of 80% HAN-water at 1.0 MPa

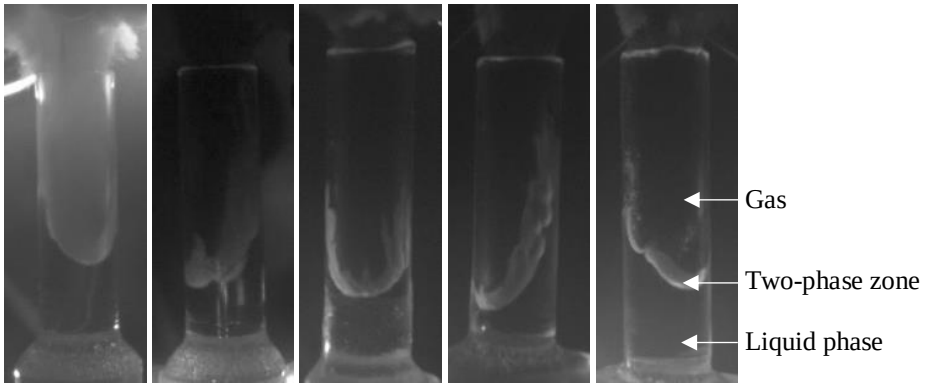

Figure 7. Combustion wave of 80% wt. HAN-water at 3.0, 4.0, 6.0, 8.0 and 10.0 MPa (left to right)

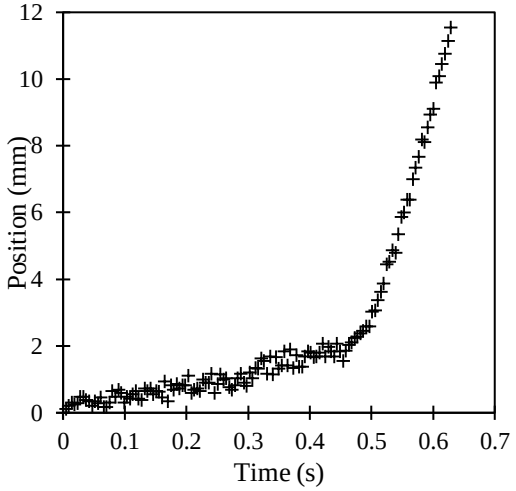

Figure 8. Position of the burning front for 80% wt. HAN-water at 1.5 MPa, showing the transition between low and high burning rate within a single test.

Each burn rate phase corresponds to a different combustion behavior observed by HSI. As shown in Figure 6, the low burn rate region presents a stratified combustion structure, with a liquid phase, a two-phase area and an opaque gas phase. The two-phase area is thin with large bubbles being formed, resulting in an unstable interface with highly variable shape. The high burn rate region at higher pressure appears to have a two-phase zone with many small bubbles, as shown in Figure 7. The interface between the liquid phase and the two-phase area is stable and adopts a highly curved profile while the interface between the gas and two-phase area is highly unstable. High-speed images indicate that the thickness of the two-phase area decreases when pressure increases, as shown in Figure 7. Unfortunately, the rapidly changing gas interface does not allow for an easy measurement of two-phase area thickness. At the lower end of the high burn rate pressure range, no interface between the gas and two-phase area was observed. The intermediate burn rate region corresponds to a transition between the low and high burn rate. Specifically, both behaviors can be observed in the same burn event, as shown in Figure 8.

C. [Emim][EtSO$_4$]-HAN Linear Burn Rate

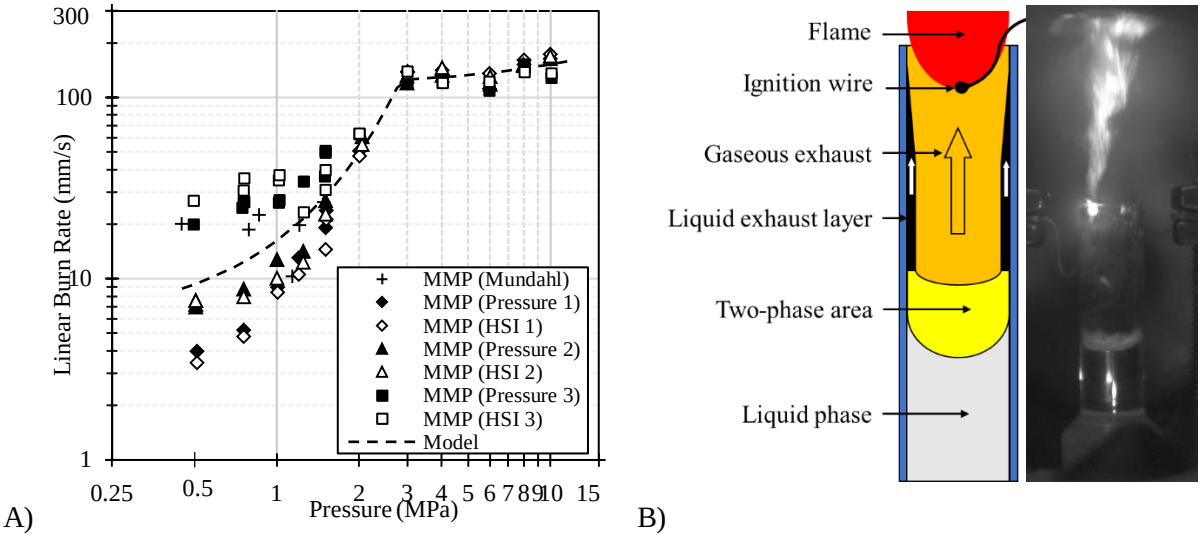

Figure 9. (A) Linear burn rate of 59%HAN-41%[Emim][EtSO$_4$] multimode propellant, also with data from Mundahl et al. [12], and (B) combustion structure of 59%HAN-41%[Emim][EtSO$_4$] at 1.0 MPa

The burn rate of 59%HAN-41%[Emim][EtSO$_4$] propellant is presented in Figure 9A, along with data from Mundahl et al. [12], who also investigated this propellant. A low-to-high pressure transition is observed between 0.5 and 3.0 MPa, and an approximately constant burn rate of 140 mm/s at the high end (3.0-10.0 MPa) of the pressure range. There is no abrupt change in slope during the transition. There is good internal agreement between the measurements in the 2.0-10.0 MPa range, with a maximum relative standard deviation of 11%. There is significant spread in the data in the 0.5-1.5 MPa range, increasing as pressure decreases, with a maximum standard deviation of 75% for 0.5 MPa and an average standard deviation of 31% for the entire range. This variation is not entirely random, it is due to the higher burn rates measured for one of the three test series (Series 3) while the other two test series show better agreement between each other. The average burn rate of Series 3 between 0.5 and 1.5 MPa is 32.32 ± 2.03 mm/s, while Series 1 and 2 average to 11.74 ± 1.38 mm/s. The standard deviation of the two coherent series is 12.5% on average, with a maximum of 28%. The reason behind this difference is not fully understood. It may be possible that variations during the preparation of the propellant could be the cause, as Series 3 data were acquired using a different batch of propellant. Previous measurements of linear burn rate by Mundahl [12] lie between the values of Series 3 and Series 1 and 2, without fitting well with either. The average relative gap between pressure and HSI measurement is 15% with a larger gap observed at low pressure (<2.0 MPa) likely due to smoke interference, which obscures the HSI and thus prevents the burn rate from being measured during the entirety of the burn. In the 0.5-3.0 MPa range, the data show good agreement with an exponential model, exhibiting a coefficient of determination of 0.625 for $r_b = 5.35e^{1.11P}$. When considering Series 1 and 2 only, the correlation increases to 0.934 for $r_b = 2.63e^{1.37P}$. Between 3.0 and 10.0 MPa, a slightly increasing linear trend is observed, with a correlation of 0.315 for $r_b = 3.84P + 114$. For Series 1 and 2 only, a better fit is observed for a polynomial expression $r_b = 1.482P^2 - 14.67P + 168$ with a coefficient of correlation of 0.722.

The combustion structure of 59%HAN-41%[Emim][EtSO$_4$] does not fundamentally change with pressure, and is shown and illustrated in Figure 9B. It includes a liquid phase, a two-phase area visible as a white foam where the bulk

of HAN decomposition is assumed to happen, and an exhaust area. In the exhaust area, the walls of the propellant holder are covered in a layer of unburned propellant, assumed to be partially decomposed [Emim][$EtSO_4$] entrained by the gaseous exhaust flow. HSI suggests that the propellant undergoes staged combustion, as the exhaust produces a bright flame that is initiated by and emanates from the hot remnant of the ignition wire, as shown in Figure 9B. This behavior is common for high activation energy fuel mixtures reported in the literature. At higher pressure (>2.0 MPa), the end of the combustion is signaled by a rapid descent of the flame down the propellant holder, seen in Figure 10A.

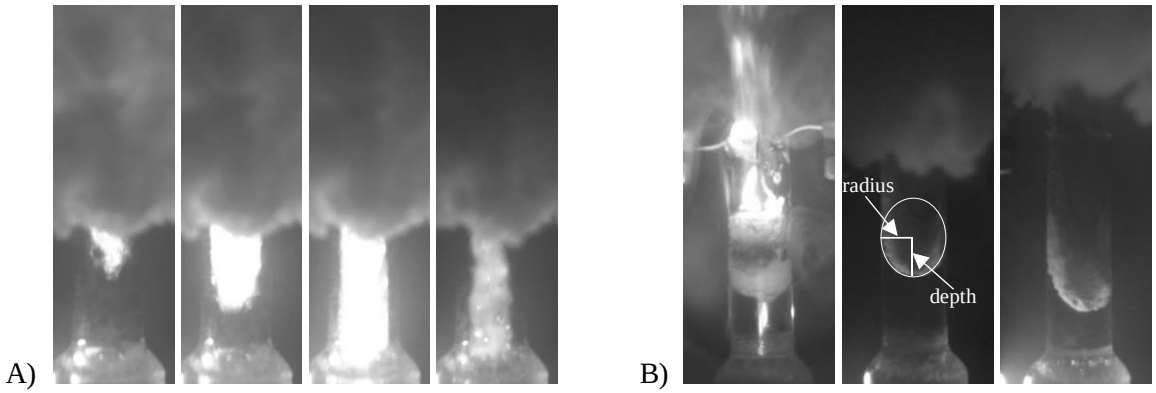

Figure 10. (A) End-of-burn flame progression of 59%HAN-41%[Emim][$EtSO_4$] at 8.0 MPa and (B) two-phase interface at 1.0 MPa, 2.0 MPa and 10.0 MPa (left to right)

At lower pressure (<1.0 MPa) the flame is not observed, and the layer of unburned propellant appears to follow a pulsing vertical movement. The authors hypothesize that the upward entrainment of the exhaust gases is not large enough to counter the weight of the unburned liquid layer, which causes it to fall. When the liquid layer contacts the hot two-phase area, it reacts, causing an increase in gas generation which creates a strong pulse of exhaust gas. This pulse entrains the layer upward, continuing the cycle. Possible causes for this increase in reactivity include decomposition of residual HAN in the falling layer or vaporization of [Emim][$EtSO_4$] decomposition products due to increasing temperature in the two-phase area. The interface between the two-phase area and the liquid area displays a meniscus with a stronger curvature at high burn rate, similar to 80% HAN-water propellant. The radius-to-depth ratio of the meniscus, as defined in Figure 10B, decreases from 1.41 at 1.0 MPa to 1.01 at 2.0 MPa and 0.74 at 10.0 MPa. This interface is corrugated, with a large amount of small-scale instabilities due to bubbling**.**

IV. Discussion

In this section, the results of the current study will be compared with literature. Burn rate and HSI observation of benchmark propellants nitromethane and 80% wt. HAN-water show excellent qualitative and quantitative agreement with literature data. The 59%HAN-41%[Emim][$EtSO_4$] propellant is compared with other HAN-fuel mixtures described in the literature. This propellant is found to have burn rate and visual burning characteristics very similar to other HAN-fuel mixtures.

A. Nitromethane burn rate

Nitromethane linear burn rate has been well-documented in the past. Boyer and Kuo[30] identified a combustion regime in the 3.0-15.0 MPa range in which the linear burn rate exhibits an almost linear relationship with pressure, with further studies confirming these results [27][28][31]. The average linear burn rates measured in this study are plotted in Figure 11 alongside earlier studies using a similar experimental setup (quartz strand burner). The results show good agreement with previous data. Relative to the least-square linear regression of literature data, the averages of HSI-based results over the 3.0 to 11.0 MPa range and the average of pressure-based results in the 3.0 to 9.0 MPa range have respective coefficients of determination of 0.996 and 0.978.

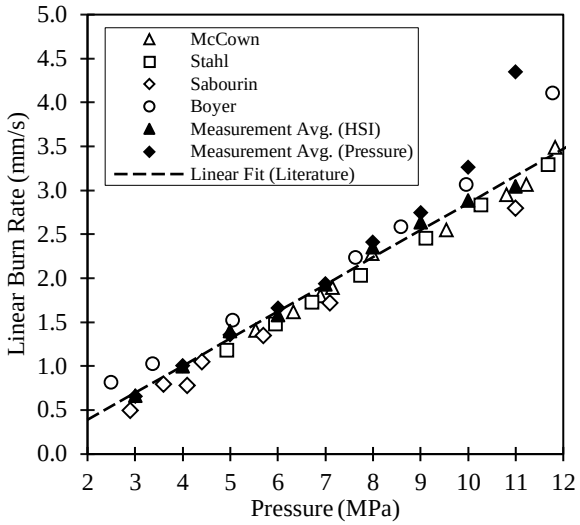

Figure 11. Comparison of nitromethane linear burn rates with literature results [27][28][30]–[32].

B. 80% wt. HAN-water burn rate

HAN-water burn rate results from numerous literature sources are provided in Figure 12A. Katsumi [29] found that HAN concentration has an impact on the pressure range at which the transition occurs and on the maximum burn rate of the propellant. He showed that the burn rate of HAN-water depends primarily on pressure and HAN content, with 3 regions being identified: low burn rate (<10 mm/s), high burn rate (>100 mm/s), and intermediate burn rate. This last region corresponds to a transition between low and high burn rate. For concentrations below 80% wt., the transition is abrupt and takes place between 1 and 3 MPa. Above this limit, the transitions take place in an increasingly larger pressure range, with Kondrikov[33] showing that pure HAN crystals follow a $r_b = aP^n$ law typical of solid propellants in the 1.0-10.0 MPa range. A HAN concentration of 80% wt. corresponds to the maximum linear burn rate, as shown in Figure 12A.

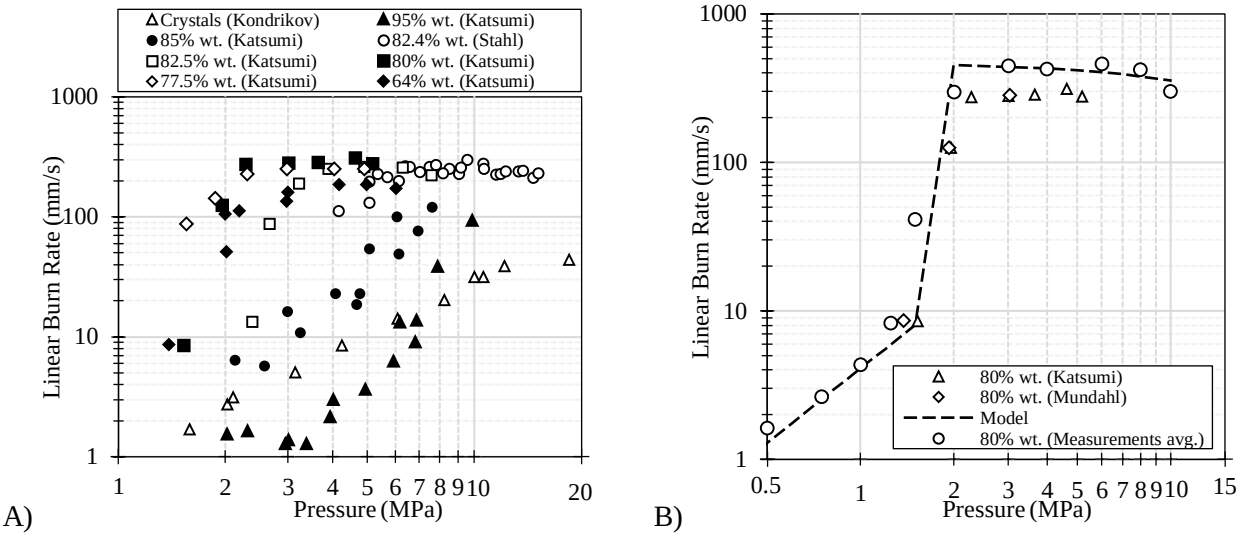

Figure 12. (A) Literature results for HAN-water linear burn rate [28][29][33], and (B) comparison of our 80% wt. HAN-water burn rate with literature data [12][34]

In the high burn rate region, the linear burn rate is approximately constant with pressure for all HAN mixtures. This description was confirmed by Stahl [28] in his investigation of the burn rate of 82.4% wt. HAN-water propellant and agrees with the behavior of 80% wt. HAN-water observed in this study. Our results are presented alongside literature data for 80% wt. HAN concentration in Figure 12B. While demonstrating transition at the same pressure as previous studies (1.5-2.0 MPa), the measurements displays a significantly higher linear burn rate above 2.0 MPa. Katsumi reports an average linear burn rate of 288 mm/s between 2.27 and 5.17 MPa while this study found an average

of 424 ± 11 mm/s between 3.0 and 6.0 MPa, a 47% increase. This discrepancy is not fully understood. A potential cause could be the use of a propellant holder with a smaller internal diameter (6 mm for this study vs 12 mm for Katsumi), which might cause different hydrodynamic mode to be present during the combustion and thus change the burn rate.

C. HAN-fuel mixture burn rate

HAN-fuel mixtures have been extensively studied, first in the context of liquid gun propellant (LGP) research and later as a substitute for hydrazine in space propulsion application. Suitable fuel components, which must be ionic or highly polar to ensure miscibility with HAN, include nitrate salts of aliphatic amines (triethanolammonium nitrate (TEAN)[35] and ethyliammonium nitrate (EAN)[33] in particular), zwitterions (amino-acids such as choline[11] and glycine[36]), and alcohols (methanol[34], [36]), with water being a frequent additive. The results from these studies are presented in Figure 13. From Figure 13A, in the 1.0-10.0 MPa pressure range, Chang explored the burn rate of XM46, a mixture of 63.2% wt. HAN, 20% wt. triethanolammonium nitrate (TEAN) and 16.8 % water, first developed as an LGP, as well as HAN-glycine-water (HANGLY26) and HAN-methanol-water mixtures (HAN269MEO15 and HAN284MEO17). Chang found that HAN-based propellant can exhibit staged combustion, particularly with high activation energy fuel such as TEAN [36]. In a staged decomposition, HAN undergoes decomposition first, then TEAN, then the decomposition products react together, creating a bright flame far above the decomposition front of the propellant. In the case of HAN-[Emim][$EtSO_4$], HSI suggests that the propellant also undergoes staged combustion, as the exhaust produces a bright flame that appears when initiated by the hot remnant of the ignition wire, as shown in Figure 9B. Chang also reports that a pulsing behavior can be observed in the burn rate of HAN-methanol mixtures under 1.14 MPa[36], similar to the low-pressure behavior of HAN-[Emim][$EtSO_4$] under 1.0 MPa.

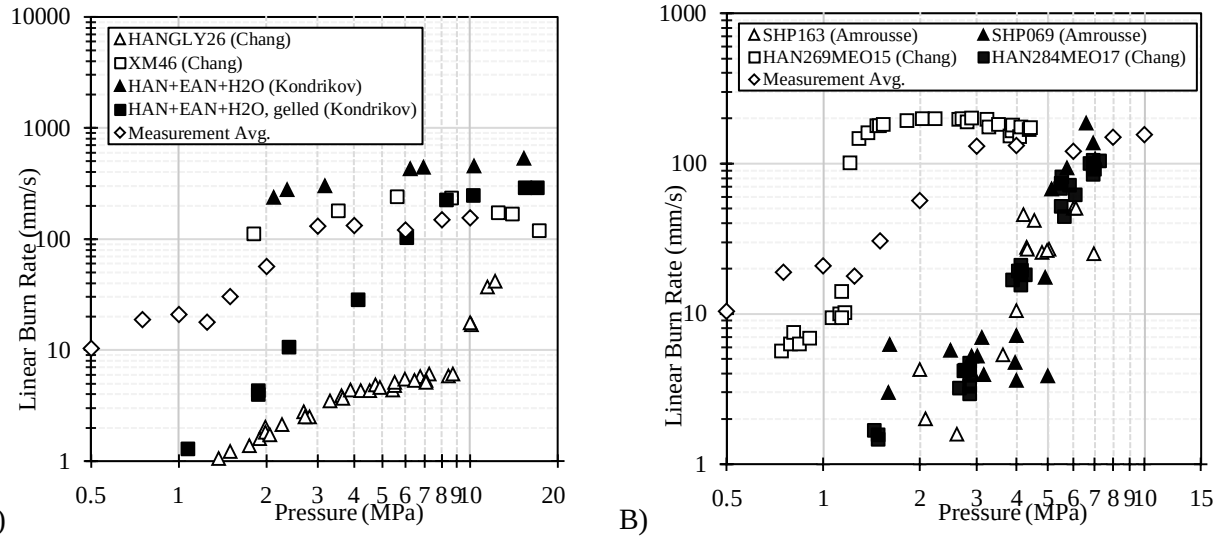

Figure 13. Comparison of 59%HAN-41%[Emim][$EtSO_4$] propellant linear burn rate with (A) HAN-amine propellants [33][35][36], and (B) HAN-methanol propellants [34][36].

Methanol has been found to decrease linear burn rate in HAN-fuel mixtures [37], a result confirmed by Amrousse [34]. The lower burn rate of methanol-based propellants can be explained by the boiling point-burn rate model proposed by Katsumi [29] for HAN-water mixture, as methanol lower the boiling temperature of the propellant [37]. A lower boiling temperature means that the propellant will stay in the low burn rate mode in a wider pressure range, delaying the transition to high burn rate. The comparison of the burn rates of HAN269MEO15 (14.91% water, 15.39% methanol) and HAN284MEO17 (4.86% water, 17.86% methanol) in Figure 13B clearly demonstrate the transition-delaying effect of a higher methanol-to-water content.

The burn rate of HAN with ethanolammonium nitrate (EAN), a room-temperature ionic liquid, has been reported by Kondrikov [33] both in gelled and conventional liquid form. A significantly higher burn rate is observed for non-gelled propellant, which indicates that hydrodynamic effects have a strong influence on burn rate. In addition, it is observed that the propellants with the highest water content (notably HAN269MEO15 and HANGLY26) have the most abrupt transitions from low to high burn rate. Table 1 shows the composition of these propellants. Comparing this composition with the burn rate trends of Figure 13 indicates that higher water content gives rise to more abrupt transition from low to high burn rate. In contrast, low-water (<10%) propellants do not have obvious discontinuities

in their burn rate vs. pressure, exhibiting a wide transition zone. This is similar to the behavior observed in HAN-water solution (Figure 12), with the more diluted mixtures have more abrupt transitions than concentrated ones. The burn rate of HAN-[Emim][$EtSO_4$] is presented in Figure 13 along with the literature results for HAN-fuel propellants. The smooth low-to-high burn rate is consistent with the absence of water in its composition. The range and trend of burn rates measured here (1-200 mm/s) are similar to those of other HAN-fuel mixtures.

Table 1. Literature Propellant Composition

Propellant	Water content (%)	HAN Content (%)	Other (%)
HANGLY26	26	60	14
XM46	16.8	63.2	20
HAN269MEO15	14.91	69.7	15.39
SHP069	6.9	81.9	11.21
SHP163	6.20	73.64	20.16
Kondrikov	5	57.5	37.5
HAN284MEO17	4.89	77.25	17.86

V.Conclusion

The linear burn rates of nitromethane, 80% wt. HAN-water, and 59%HAN-41%[Emim][$EtSO_4$] have been measured and their combustion behavior has been documented through high-speed imaging (HSI). The results obtained for nitromethane agree well with the literature with a coefficient of determination above 0.97, while 80% wt. HAN-water shows combustion behavior and burn rate trends similar to previous studies, albeit with a consistently higher burn rate. In particular, it is found that 80% wt. HAN-water burn rate follows a power law $r_b = 4.09P^{1.66}$ between 0.5 and 1.5 MPa and a linear law $r_b = 478 - 12.30P$ between 2.0 and 10.0 MPa. The combustion structure of 59%HAN-41%[Emim][$EtSO_4$] was characterized with a liquid phase, two-phase area and an exhaust area including a liquid film layer of unburned propellant and a stream of hot decomposition gases undergoing staged combustion. Its burn rate appears to follow an exponential law $r_b = 5.35e^{1.11P}$ between 0.5 and 3.0 MPa and a linear law $r_b = 114 + 3.84P$ between 3.0 and 10.0 MPa. These results show behavior that is similar to other HAN-fuel mixtures previously studied in the literature. A large variability in the low-pressure linear burn rate was observed with a maximum standard deviation of 75% at 0.5 MPa. Further study of HAN-ionic liquid monopropellants is needed to characterize the influence of ionic liquid properties and proportions on burn rate and offer a suitable model for their combustion. The temperatures in the two-phase and gas-phase regions, and analysis of the composition of unburned propellant, would be useful to characterize the thermochemical behavior of the propellant. The influence of preparatory routes on HAN-ionic liquid combustion behavior must also be investigated.

References

[1] C. A. Kluever, "Spacecraft optimization with combined chemical-electric propulsion," *J. Spacecr. Rockets*, 1995.

[2] C. A. Kluever, "Optimal Geostationary Orbit Transfers Using Onboard Chemical-Electric Propulsion," *J. Spacecr. Rockets*, vol. 49, no. 6, pp. 1174–1182, 2012.

[3] S. R. Oleson, R. M. Myers, C. A. Kluever, J. P. Riehl, and F. M. Curran, "Advanced Propulsion for Geostationary Orbit Insertion and North-South Station Keeping," *J. Spacecr. Rockets*, vol. 34, no. 1, pp. 22–28, 1997.

[4] T. Rexius and M. Holmes, "Mission Capability Gains from Multi-Mode Propulsion Thrust Profile Variations for a Plane Change Maneuver," vol. 298, no. 0704, 2012.

[5] S. P. Berg and J. L. Rovey, "Assessment of Multimode Spacecraft Micropropulsion Systems," *J. Spacecr. Rockets*, vol. 54, no. 3, pp. 592–601, 2017.

[6] B. R. Donius and J. L. Rovey, "Ionic Liquid Dual-Mode Spacecraft Propulsion Assessment," *J. Spacecr. Rockets*, 2011.

[7] S. P. Berg and J. L. Rovey, "Assessment of Imidazole-Based Ionic Liquids as Dual-Mode Spacecraft Propellants," *J. Propuls. Power*, 2013.

[8] S. Berg, J. Rovey, B. Prince, S. Miller, and R. Bemish, "Electrospray of an Energetic Ionic Liquid Monopropellant for Multi-Mode Micropropulsion Applications," *51st AIAA/SAE/ASEE Joint Propulsion*

Conference. AIAA Paper 2015-4011, 2015.
[9] Y.-C. Chao, G.-B. Chen, C.-J. Hsu, T.-S. Leu, C.-Y. Wu, and T.-S. Cheng, "Operational characteristics of catalytic combustion in a platinum microtube," *Combust. Sci. Technol.*, vol. 176, no. 10, pp. 1755–1777, 2004.
[10] F. G. Kidd, N. R. Taylor, and K. M. Lemmer, "Decomposition of hydroxylammonium nitrate in a low pressure flowing thermal capillary system," *J. Mol. Liq.*, vol. 262, pp. 396–404, 2018.
[11] A. J. Mundahl *et al.*, "Characterization of a Novel Ionic Liquid Monopropellant for Multi-Mode Propulsion," no. July, pp. 1–20, 2017.
[12] A. J. Mundahl, S. P. Berg, and J. L. Rovey, "Linear burn rates of monopropellants for multi-mode micropropulsion," in *52nd AIAA/SAE/ASEE Joint Propulsion Conference, 2016*, 2016.
[13] V. Hruby, M. Gamero-Castaño, P. Falkos, and S. Shenoy, "Micro Newton colloid thruster system development," *27th Int. Electr. Propuls. Conf.*, pp. 01–281, 2001.
[14] D. Spence *et al.*, "Electrospray Propulsion Systems for Small Satellites and Satlets," pp. 1–7, 2013.
[15] Y. Chiu and R. A. Dressler, "Ionic Liquids for Space Propulsion," no. January, pp. 138–160, 2009.
[16] S. P. Berg and J. Rovey, "Decomposition of a Double Salt Ionic Liquid Monopropellant in a Microtube for Multi-Mode Micropropulsion Applications," *53rd AIAA/SAE/ASEE Joint Propulsion Conference*. American Institute of Aeronautics and Astronautics, 2017.
[17] R. L. Sackheim and R. K. Masse, "Green propulsion advancement: challenging the maturity of monopropellant hydrazine," *J. Propuls. Power*, vol. 30, no. 2, pp. 265–276, 2014.
[18] A. S. Gohardani *et al.*, "Green space propulsion: Opportunities and prospects," *Prog. Aerosp. Sci.*, vol. 71, pp. 128–149, 2014.
[19] P. S. George, B. Oscar, and 7th, *Rocket Propulsion Elements*. New York: Wiley, 2001.
[20] L. Courthéoux, D. Amariei, S. Rossignol, C. Kappenstein, N. Pillet, and M. Ford, "Thermal and catalytic decomposition of HNF and HAN-based propellants," in *ESA Special Publication*, 2004, vol. 557.
[21] K. Anflo and R. Möllerberg, "Flight Demonstration of New Thruster and Green Propellant Technology on the PRISMA Satellite," *Acta Astronaut.*, vol. 65, no. 9, pp. 1238–1249, 2009.
[22] M. Farshchi, V. Vaezi, and B. D. Shaw, "Studies of Han-based monopropellant droplet combustion," *Combust. Sci. Technol.*, vol. 174, no. 7, pp. 71–97, 2002.
[23] N. Wingborg, C. Eldsäter, and H. Skifs, "Formulation and characterization of ADN-based liquid monopropellants," in *ESA Special Publication*, 2004, vol. 557.
[24] R. A. Spores, "GPIM AF-M315E Propulsion System," no. July 2013, pp. 1–10, 2015.
[25] K. Anflo and B. Crowe, "In-Space Demonstration of an ADN-based Propulsion System," no. August, pp. 1–14, 2012.
[26] W. C. Warren and D. E. L. Peterson, "Experimental Techniques for the Study of Liquid Monopropellant Combustion," Texas A&M University, 2012.
[27] K. W. McCown, A. R. Demko, and E. L. Petersen, "Experimental Techniques to Study Linear Burning Rates of Heterogeneous Liquid Monopropellants," *J. Propuls. Power*, 2014.
[28] J. Mac Stahl and E. L. Petersen, "Analysis of Hydroxylammonium Nitrate Burning Rates," Texas A&M University, 2017.
[29] T. Katsumi, K. Hori, R. Matsuda, and T. Inoue, "Combustion Wave Structure of Hydroxylammonium Nitrate Aqueous Solutions," *46th AIAA/ASME/SAE/ASEE Joint Propulsion Conference & Exhibit*. AIAA Paper 2010-6900, 2010.
[30] E. Boyer and K. Kuo, "High-pressure combustion behavior of nitromethane," in *35th Joint Propulsion Conference and Exhibit*, American Institute of Aeronautics and Astronautics, 1999.
[31] J. L. Sabourin, R. A. Yetter, and V. S. Parimi, "Exploring the Effects of Nanostructured Particles on Liquid Nitromethane Combustion," *J. Propuls. Power*, vol. 26, no. 5, pp. 1006–1015, 2010.
[32] S. Kelzenberg, N. Eisenreich, W. Eckl, and V. Weiser, "Modelling Nitromethane Combustion," *Propellants, Explos. Pyrotech.*, vol. 24, no. 3, pp. 189–194, 1999.
[33] B. N. Kondrikov, V. E. Annikov, V. Y. Egorshev, and L. T. De Luca, "Burning of hydroxylammonium nitrate," *Combust. Explos. Shock Waves*, vol. 36, no. 1, pp. 135–145, 2000.
[34] R. Amrousse, T. Katsumi, N. Azuma, and K. Hori, "Hydroxylammonium nitrate (HAN)-based green propellant as alternative energy resource for potential hydrazine substitution: From lab scale to pilot plant scale-up," *Combust. Flame*, vol. 176, no. Supplement C, pp. 334–348, 2017.
[35] Y.-P. P. Chang, E. Boyer, and K. K. Kuo, "Combustion Behavior and Flame Structure of XM46 Liquid Propellant," *J. Propuls. Power*, vol. 17, no. 4, pp. 800–808, 2008.
[36] Y.-P. Chang, "Combustion Behavior of HAN-Based Liquid Propellants," The Pennsylvania State University, College Park, PA, 2002.

[37] Y. P. Chang, J. K. Josten, B. Q. Zhang, and K. Kuo, "Combustion Characteristics of Energetic HAN/Methanol Based Monopropellants," *38th AIAA Joint Propulsion Conference*, vol. AIAA Paper. 2002.